Journal of Environmental Chemical Engineering 4 (2016) 681–694

Contents lists available at ScienceDirect

Journal of Environmental Chemical Engineering

journal homepage: www.elsevier.com/locate/jece

Sorptive removal of arsenite [As(III)] and arsenate [As(V)] by fuller's earth immobilized nanoscale zero-valent iron nanoparticles (F-nZVI): Effect of Fe^0 loading on adsorption activity

Radheshyam Yadav[a], Archana Kumari Sharma[a], J. Nagendra Babu[b,*]

[a] Centre for Environmental Science and Technology, School of Environment and Earth Sciences, Central University of Punjab, Bathinda 151001, Punjab, India
[b] Centre for Chemical Sciences, School of Basic and Applied Sciences, Central University of Punjab, Bathinda 151001, Punjab, India

ARTICLE INFO

Article history:
Received 13 August 2015
Received in revised form 16 November 2015
Accepted 17 December 2015
Available online 19 December 2015

Keywords:
Arsenic adsorption
Fuller's earth
nZVI
Iron loading
Kinetics

ABSTRACT

Fuller's earth immobilized nanoscale zerovalent iron (F-nZVI 1–8) were synthesized by borohydride reduction method. The iron loading of fuller's earth immobilized nZVI was varied from 5 to 50% (w/w) in these F-nZVI 1–8. The F-nZVI 1–8 were characterized by FE-SEM–EDX, FTIR, BET, XRD and TGA. The FE-SEM analysis showed an increase in agglomeration of nZVI on the immobilized material with increase in the loading of Fe^0. F-nZVI 1–8 were studied for adsorptive removal of As(III) and As(V) from aqueous solution, with an emphasis on the effect of Fe^0 loading of adsorbent on arsenic remediation. Iron loading has a significant role in adsorption of As(III) and As(V) on F-nZVI, with increase in adsorption with optimum iron loading of 20% (w/w) on fuller's earth (F-nZVI-4). However, increase in loading above 20%, resulted in no significant increase in As(III) and As(V) adsorption. The adsorption results fitted well with Langmuir and Freundlich isotherm models and the maximum adsorption capacity of F-nZVI-4 for As(III) and As(V) were observed to be 50.08 and 91.42 mg/g, respectively. The adsorption isotherm and kinetic studies indicate a rapid removal of As(III) and As(V) from the aqueous solution in the presence of F-nZVI 1-8, with an substantially high rate of removal for arsenic with F-nZVI-4.

1. Introduction

Arsenic is a metalloid and natural constituent of earth's crust which is recognized as a one of the most ubiquitous pollutant in the environment [1] and bioaccumulate in marine life [2], threatening the life of human population [3]. Biochemical processes have resulted in the release of naturally occurring arsenic into groundwater whereas uncontrolled anthropogenic activities such as mining, fossil fuel burning, smelting of metal ores, wood preservatives and pesticide use, release arsenic directly into the environment [4]. In ground and surface water, the prevalent forms of arsenic are inorganic arsenite (AsO_3^{3-}) and arsenate (AsO_4^{3-}) [5] whereas, organic arsenical are less prevalent and formed from biomethylation processes which generally bioaccumulate in aquatic organisms [6,7]. As(III) and As(V) are both linked to energy related functions of mitochondria in a cell. As (III) has very high affinity for sulfhydryl groups in protein leading to formation of thiolated species which inhibit the enzyme activity. However, As(V) compete with phosphate and limit oxidative phosphorylation which is key to the high bond energy of ATP molecules [8]. Further, As(III) is more toxic and mobile in environment than As(V) [9], due to its existence in neutral form (H_3AsO_3) under a wide range of physiological conditions. As(V)/As (III) ratio plays a significant role in our environment. The As(V)/As (III) ratio in the environment is partly explained on the basis of pH–pE conditions, as in case of sea water it lies in the range of 10^{15}–10^{26}. However, in the marine organisms and humans this ratio is found to decrease tremendously. A primary exposure of human body to arsenic is through the consumption of contaminated water, which leads to arsenic poisoning or arsenicosis [10]. Long term exposure to arsenicals cause severe diseases such as hyperkeratosis, skin lesions, black foot diseases and cancer of the bladder, lungs, skin, kidney and liver [11,12]. Due to its significant toxicity, World Health Organization (WHO) has established 10 μg/L as the maximum contaminant level for total arsenic in potable water [12].

Various conventional technologies have been used for arsenic remediation including oxidation and reduction [13], co-precipitation [14], membrane processes [15] and ion-exchange resins[16]. Besides these techniques, adsorption [17–19] is a common technique successfully employed for water treatment of heavy metal remediation. However, oxidation and reduction, chemical

* Corresponding author.
E-mail address: nagendra.rd@gmail.com (J. N. Babu).

http://dx.doi.org/10.1016/j.jece.2015.12.019
2213-3437/

precipitation and electrochemical process of arsenic removal are ineffective, especially when the arsenic concentration in the aqueous solution is higher [20]. Ion-exchange and membrane technology are expensive when treating large quantity of water containing arsenic and they cannot be used at large scale [21]. But among these conventional processes, adsorption is more commonly used due to its easy operation and cost effectiveness, when the loaded adsorbent can be regenerated for repeated use [22]. Based on the natures association of arsenic with soil [23], hematite and pyrite, various synthetic adsorbents studied for arsenic removal include alum [24], alumina [25], manganese oxide [18,26], and hydrotalcite [27,28]. ZVI (iron filings) and iron oxides have shown a very good adsorption efficiencies for arsenic remediation by reductive-sorption and μ-oxo bridging interactions, respectively [29,30]. However, the mechanism for removal of both As(III) and As(V) by ZVI, is generally characterized by adsorption on enclosing oxide layer or by co-precipitation with Fe (II)/Fe(III) produced at the interface of the material and solution during corrosion [31,32].

In an effort to enhance the removal efficiency of iron based material, nanoscale zero-valent iron (nZVI) were developed. nZVI not only remediates arsenic but has a broad range of application in reductive removal of heavy metals [33,34], nitrite [35], trichloroethylene [36] and pesticides [37] from groundwater. However, these nZVI particles tend to get oxidized by air or water and agglomerate due to their high surface energy and intrinsic magnetic interaction, which leads to constrained chemical reactivity of the material [38]. The optimum activity of nZVI is ensured using stabilizers and/or immobilizers. Stabilizers are passivators, which reduce the interaction between the surface of nZVI and water present in the immediate environment. Alternatively, immobilizers are polymers on which the particles are entrapped and entrained, leading to lower agglomeration. Various immobilizers have been used for stabilizing and increasing activity of nZVI such as PVA microspheres [39], resins [40], multiwall carbon nanotubes [41], cellulose [42], Ca-alginate [43], chitosan [44], activated carbon [45], cation exchange membranes [46] and silica[47]. Apart from these, various aluminosilicates have been reported for the immobilization of the nZVI including zeolite [48], montmorillonite [49], kaolinite [50] and bentonite [51]. These aluminosilicate immobilized nZVI show higher efficiency for arsenic adsorption in comparison of bare nZVI [52]. Thus in the present work, fuller's earth immobilized nZVI with different iron loading were characterized and studied for their arsenic adsorption efficiency. Fuller's earth is a fine-grained, naturally occurring earthy substance that has been used in many medical and cosmetics applications. It has been used as a natural adsorbent in decontamination of dyes wastewater [53] and mercury [54]. This adsorption behaviour is attributed to large surface area and negative surface charge of fuller's earth in comparison to other aluminosilicates. Thus, in continuation of our work on immobilized nZVI for water treatment [42], study of effect of iron loading on adsorption efficiency of F-nZVI was carried out.

2. Experimental

2.1. Materials

All chemicals used including fuller's earth, anhydrous ferric chloride ($FeCl_3$), sodium borohydride ($NaBH_4$), polyethylene glycol [$HO(C_2H_4O)_nH$], methanol (CH_3OH), sodium hydroxide (NaOH) and hydrochloric acid (HCl) were of analytical grade and used directly without further purification. The stock solution of As(III) and As(V) were prepared from sodium arsenite ($NaAsO_2$), and sodium arsenate ($Na_2HAsO_4{\cdot}7H_2O$). All the solutions were prepared with type-1 water (resistivity $< 18.2\ M\Omega\,cm$; total organic content (TOC) < 10 ppb) under ambient condition.

2.2. Preparation of F-nZVI

To a suspension of fuller's earth (36 g) in 2% aqueous polyethylene glycol solution (500 mL), ferric chloride ($FeCl_3{\cdot}6H_2O$) in varied amount (2.74–27.40 g) was added and kept under stirring for 30 min. Dropwise addition of aqueous $NaBH_4$ (10 or 20% w/v) aqueous solution was carried over a period of 2 h with continuous stirring. The completion of reaction was characterized by the colourless solution and black coloured suspension settled to the bottom. Upon completion of the reduction, the black coloured precipitate is separated by Buchner filtration. The residue were washed with excess methanol to remove borohydride impurity and moisture retained on the surface of the material and resulting black solid was dried in-vacuo to furnish F-nZVI 1-8 with 5–50% (w/w) iron loading on fuller's earth. This material was stored in tight capped containers to prevent the aerial oxidation prior to characterization and adsorption experiment.

2.3. Characterization

The specific surface area of fuller's earth and F-nZVI were measured by BET-N_2 adsorption method (Brunauer–Emmett–Teller) using Micrometrics ASAP-2020, where the samples were dried with constant flow of N_2 at 60 °C for 24 h. The structure and surface morphology of fuller's earth and F-nZVI were studied by field emission-scanning electron microscope (FE-SEM) (CARL-ZEISS model Merlin Compact, Germany) operating at 4 kV equipped with energy dispersive X-ray (EDX) analyzer. The dried samples were coated with gold prior to FE-SEM analysis. The infrared transmittance spectra were obtained using BRUKER TENSOR 27 Fourier Transform Infra-Red (FTIR) spectrometer. Samples were prepared by mixing specimens with KBr powder in 1:20 (w/w) ratio, and pressing the mixture into a pellet. X-ray diffraction (XRD) pattern of fuller's earth and F-nZVI were performed on a Bruker D8 X-ray powder diffractometer with a high power Cu-Kα radioactive source ($\lambda = 0.154$ nm) at 40 kV/40 mA. Continuous scans for 2θ from 10^0 to 70^0 were collected at a scan rate of about 3°/min. The thermal properties of adsorbents were analysed using a DTA-TG apparatus (DTG-60H, Shimadzu, Japan) from 25 to 550 °C at heating rate of 10 °C/min in nitrogen atmosphere.

2.4. Adsorption experiment

Stock solution (1000 mg/L) of As(III)/As(V) were prepared. As (III)/As(V) solutions of desired concentration (20–100 mg/L) were prepared by diluting the stock solution. Adsorption studies were performed using 100 mL of arsenic solution in determinate concentration, pH of solution adjusted between 3 and 10 using HCl and NaOH, followed by the addition of 1 g/L of synthesized F-nZVI 1–8. The flasks were maintained at constant temperature of 25 ± 2 °C under shaking at 150 rpm using an incubator shaker. The solutions were filtered after 24 h using Whatman filter paper and analysed on Atomic Absorption Spectrophotometer (AAS) in flame mode. All the experiments were performed in duplicate and blank were prepared under identical experimental conditions. The amount of arsenic adsorbed on to F-nZVI was calculated using the following equation:

$$q = V\frac{C_i - C_t}{M} \quad (1)$$

where q is the mass of arsenic adsorbed, V is volume of solution and M is the mass of adsorbent. C_i and C_t are initial and final arsenic concentration at time t, respectively.

3. Results and discussion

3.1. Synthesis

Fuller's earth immobilized nZVI 1–8 were synthesized by $NaBH_4$ reduction method as given in Scheme 1. PEG was used as stabilizer for the reduced Fe^0. However, it was observed that in case of F-nZVI 6–8 reduction with 10% $NaBH_4$ (w/v) yields product with poor nZVI stability and material oxidizes during filtration and drying. Thus, synthesis of F-nZVI 6–8 was carried out with 20% $NaBH_4$ solution to yield black coloured material, which was stable in air. Thus, it indicates that the F-nZVI stability decreases with increase in the loading of the material. The iron loading of F-nZVI 1–8 were analysed by phenanthroline method [55]. The observed iron loading in percentage was found to significantly lie within 0.2–2% of the calculated iron loading. This indicates that all the iron were reduced and immobilized on fuller's earth surface.

3.2. Characterization

3.2.1. SEM

The surface morphology of fuller's earth and F-nZVI 2, 4, 5, 7 and 8 are shown in Fig. 1. Fuller's earth showed plate like structure with smooth surface, suitable for immobilization of nZVI. The morphology of F-nZVI 2 and 4 showed uniform particle size for nZVI with size varying in the range of 30–60 nm. The nZVI were found to be dispersed on the surface of fuller's earth. F-nZVI 2 and 4, showed dispersed nanoparticles with very less chain like agglomeration characteristic of nZVI. However, agglomeration is significantly increased in case of higher loading of iron on fuller's earth. Kim et al. have reported similar lower agglomeration of nZVI on the surface of the aluminosilicates.

The EDX analysis of fuller's earth showed the presence of various major components namely Si (32.53%), O (49.50%), Al

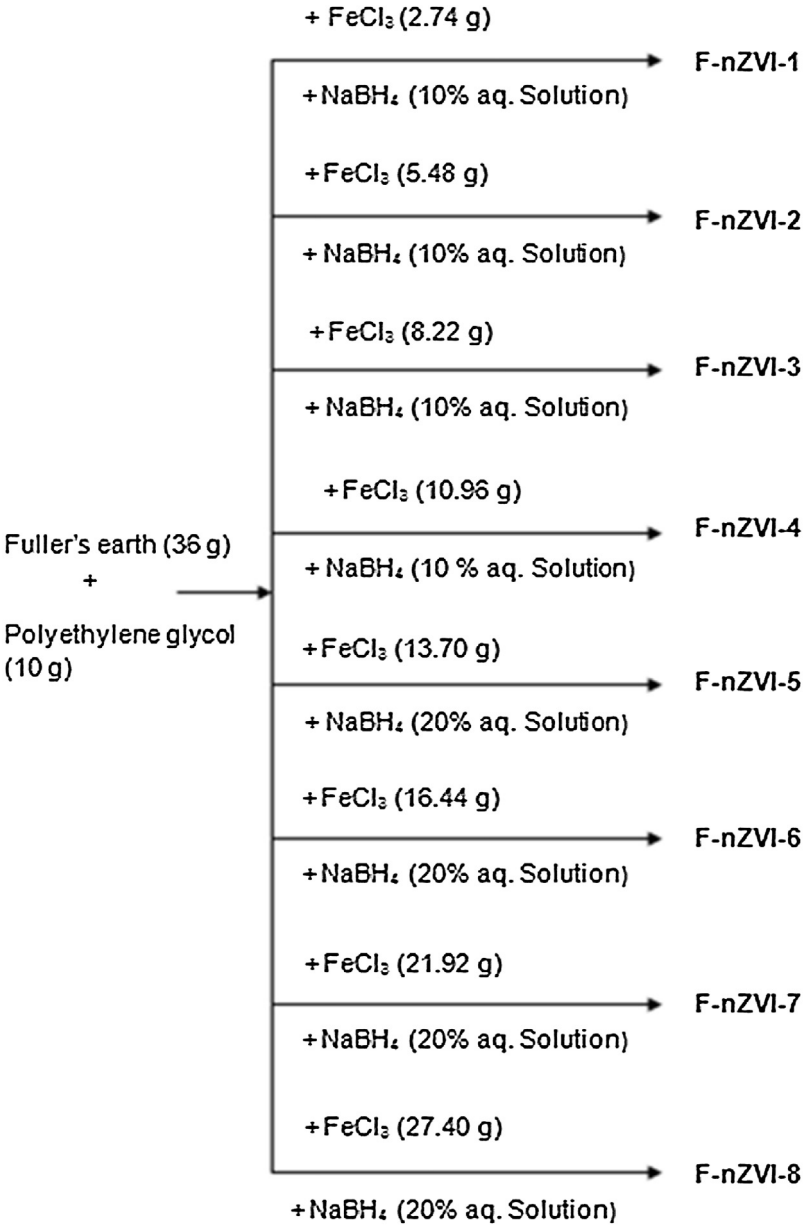

Scheme 1. Synthesis of fuller's earth immobilized nZVI (F-nZVI 1-8).

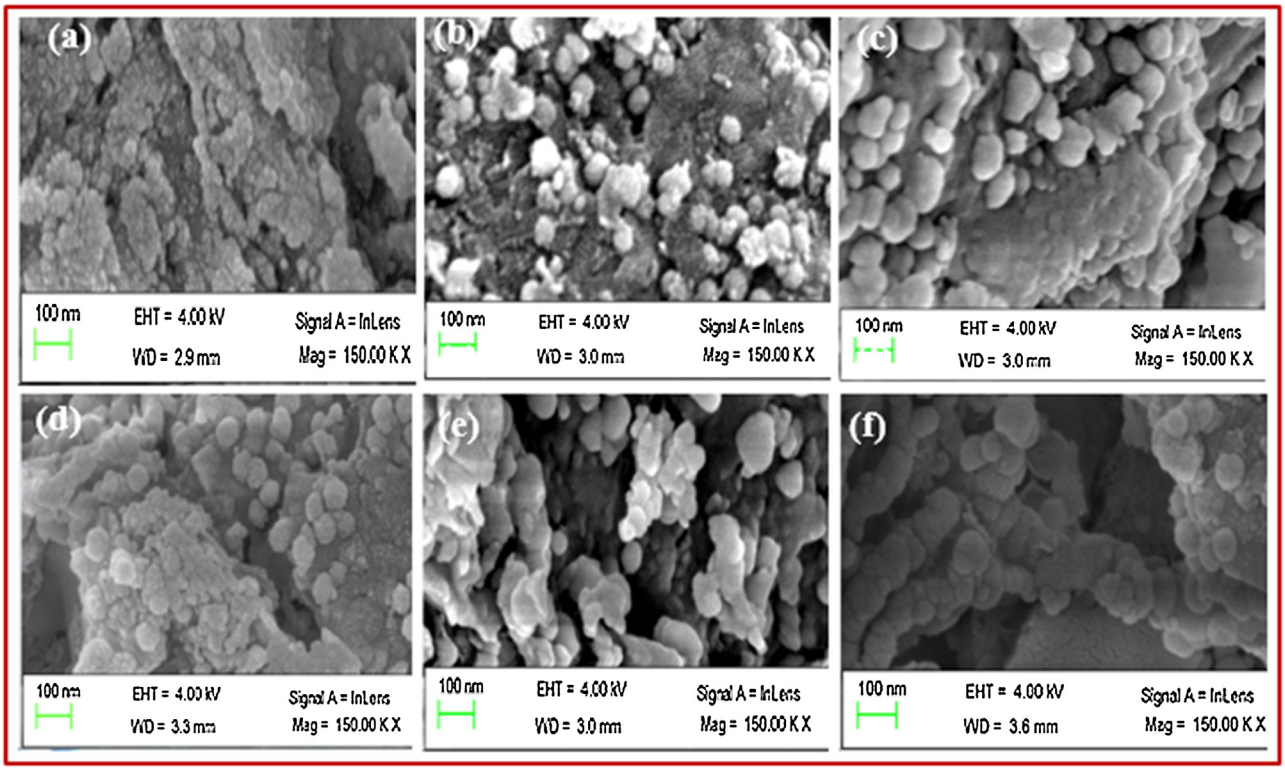

Fig. 1. SEM images of (a) fuller's earth; (b) F-nZVI-2; (c)F-nZVI-4, (d) F-nZVI-5(e) F-nZVI-7, and (f) F-nZVI-8.

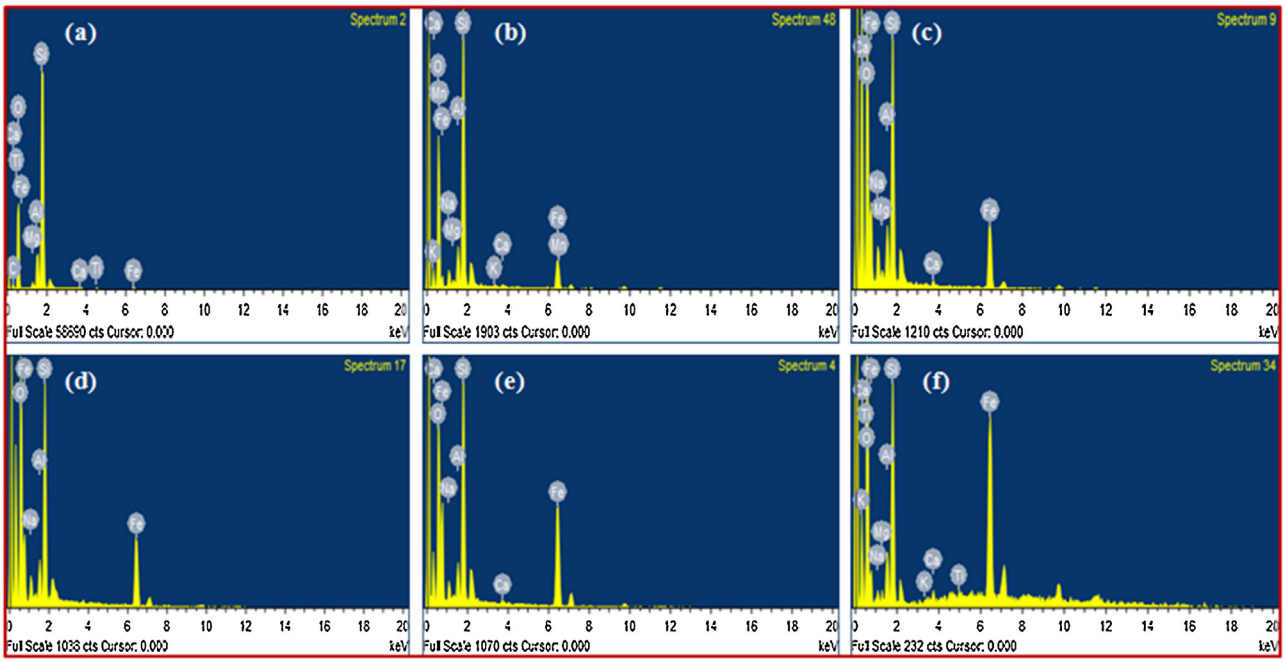

Fig. 2. EDX spectra of (a) fuller's earth; (b) F-nZVI-2; (c) F-nZVI-4, (d) F-nZVI-5(e) F-nZVI-7, and (f) F-nZVI-8.

(4.37%), and Fe (2.30%) (Fig. 2). The Al/Si ratio for fuller's earth was 1:5, which is lower in comparison to bentonite Al/Si (3:1) and kaolinite Al/Si (1:1) [56]. Similarly, iron content of fuller's earth was also observed to be higher than bentonite and kaolinite. Upon immobilization of Fe^0 on the fuller's earth surface, there is an increase in iron% of the F-nZVI samples as observed in the EDX spectra. Thus, SEM–EDX study of the F-nZVI-4 showed the composition, whereby a significant increase in the iron content of the material was observed.

SEM–EDX analysis of the As(III) and As(V) adsorbed F-nZVI prepared by treatment of F-nZVI (1 g/L) with arsenic solution (100 mg/L) under optimum pH of 3 and 8, respectively, were also carried out to establish the sorption phenomena (Figs. 3 and 4). Upon adsorption of arsenic onto the surface of F-nZVI, the SEM analysis showed an increase in the size of the immobilized

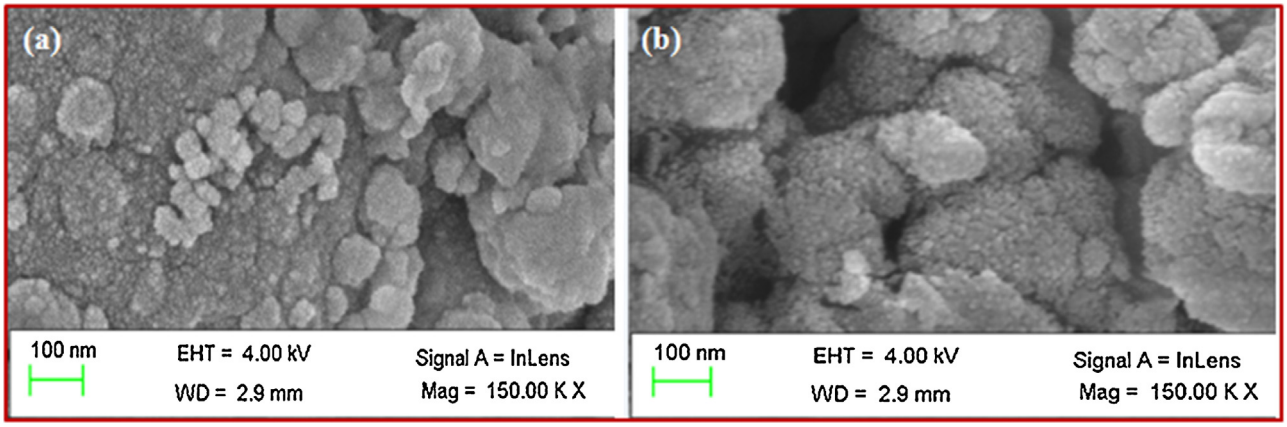

Fig. 3. SEM images of (a) As(III) and (b) As(V) adsorbed on F-nZVI-4.

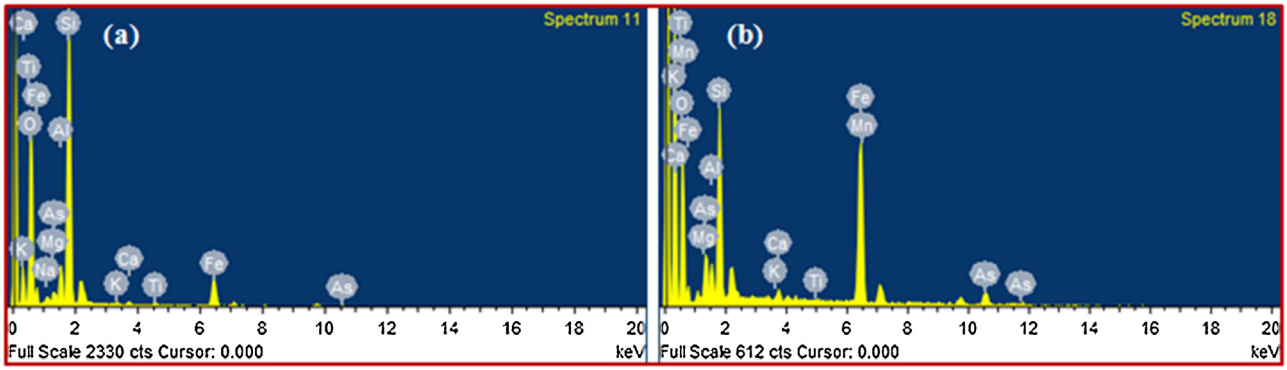

Fig. 4. EDX spectra of (a) As(III) and (b) As(V) adsorbed on F-nZVI.

nanomaterial upto 88.64–115.2 nm. This is accounted to the formation of iron oxide and iron oxide adsorbed oxo-anion complex. F-nZVI showed shape deformation from spherical to ellipsoidal upon adsorption of arsenic. The EDX analysis of arsenic adsorbed F-nZVI showed the presence of As(III) and As(V) upto a maximum concentration of 7.93%, which indicates significant adsorption of arsenic on to the surface of F-nZVI.

3.2.2. BET

The specific surface area, pore volume and mean pore diameter of the fuller's earth and F-nZVI-1, 2 and 4 were determined using BET-N_2 adsorption–desorption isotherm analysis (Fig. 5). The isotherm curve of fuller's earth and F-nZVI exhibit type-II isotherm with hysteresis loop in the P/P_o range 0.5–0.9, resulting in uniformly mesoporous structure [57]. The specific surface area (S_{BET}) for the fuller's earth, F-nZVI 1, 2 and 4, was determined to be 230, 73.54, 75.47 and 108.17 m^2/g, respectively (Table 1). The BET surface area of F-nZVI 1, 2 and 4, calculated based on the nZVI density and particle size (as determined using SEM) was 218.84, 213.93 and 185.38 m^2/g, respectively (Table 1). Thus, the immobilized nZVI significantly lowered the specific surface area and pore volume of fuller's earth. Further, this decrease in specific surface area and pore volume shows that the mesopores of fuller's earth were blocked by nZVI during the immobilization process.

The mean pore diameter of fuller's earth was 6.7 nm. Upon loading of iron (5% Fe loading) on to fuller's earth, the mean pore diameter increases from 6.7 to 8.1 nm. When increasing the loading of iron from 5 to 10 and 20%, the mean pore diameter of the material changed to 8.4 and 7.7 nm, respectively, which suggests significant blocking of the surface pores of fuller's earth being achieved at 5% loading of nZVI. Besides this, there is a significant increase in pore volume of F-nZVI-4 than F-nZVI-2. This significant increase with decrease in the pore diameter indicates a substantial aggregation in F-nZVI-4.

3.2.3. FTIR

The possible interaction between fuller's earth and nZVI particles as well as the changes in the functional group of F-nZVI after As(III) and As(V) adsorption were identified by FTIR spectroscopy. Fig. 6 represents the FTIR spectra of fuller's earth, F-nZVI-4, As(III) and As(V) adsorbed F-nZVI-4. The spectrum of fuller's earth in Fig. 6a shows absorption bands centred at 3434, 1635, 1050 and 796 cm^{-1} due to the H—O—H stretching of physiosorbed water on the surface of fuller's earth, Si—O—Si stretching and Si—O bond, respectively [58]. The FTIR spectrum of F-nZVI-4, is characterized by shift and appearance of new absorption bands due to the iron loading and its interaction with the surface of fuller's earth (Fig. 6b). The stretching band of O—H group at 3434 cm^{-1} in fuller's earth shifts to 3468 cm^{-1} upon loading of nZVI. This suggests a strong interaction between O—H moieties in fuller's earth with the surface of nZVI, as indicated by the shift in the adsorption band due to hydroxyl moieties. Appearance of new adsorption band at 1356 cm^{-1} is characteristic of nZVI loading on the fuller's earth surface [59].

The FTIR spectra of F-nZVI-4 upon As(III) and As(V) adsorption showed significant change (Fig. 6c and d). The absorption band due to hydroxyl moiety of F-nZVI-4 was observed at 3434 cm^{-1}, which was broadened upon As(III) adsorption. In contrast, upon adsorption of As(V), two absorption bands were observed corresponding to the hydroxyl moiety at 3620 and 3715 cm^{-1}. Appearance of a new absorption band at 2310 cm^{-1} (OH stretching) upon As(V) adsorption, shows that the hydroxyl moieties play a vital role in

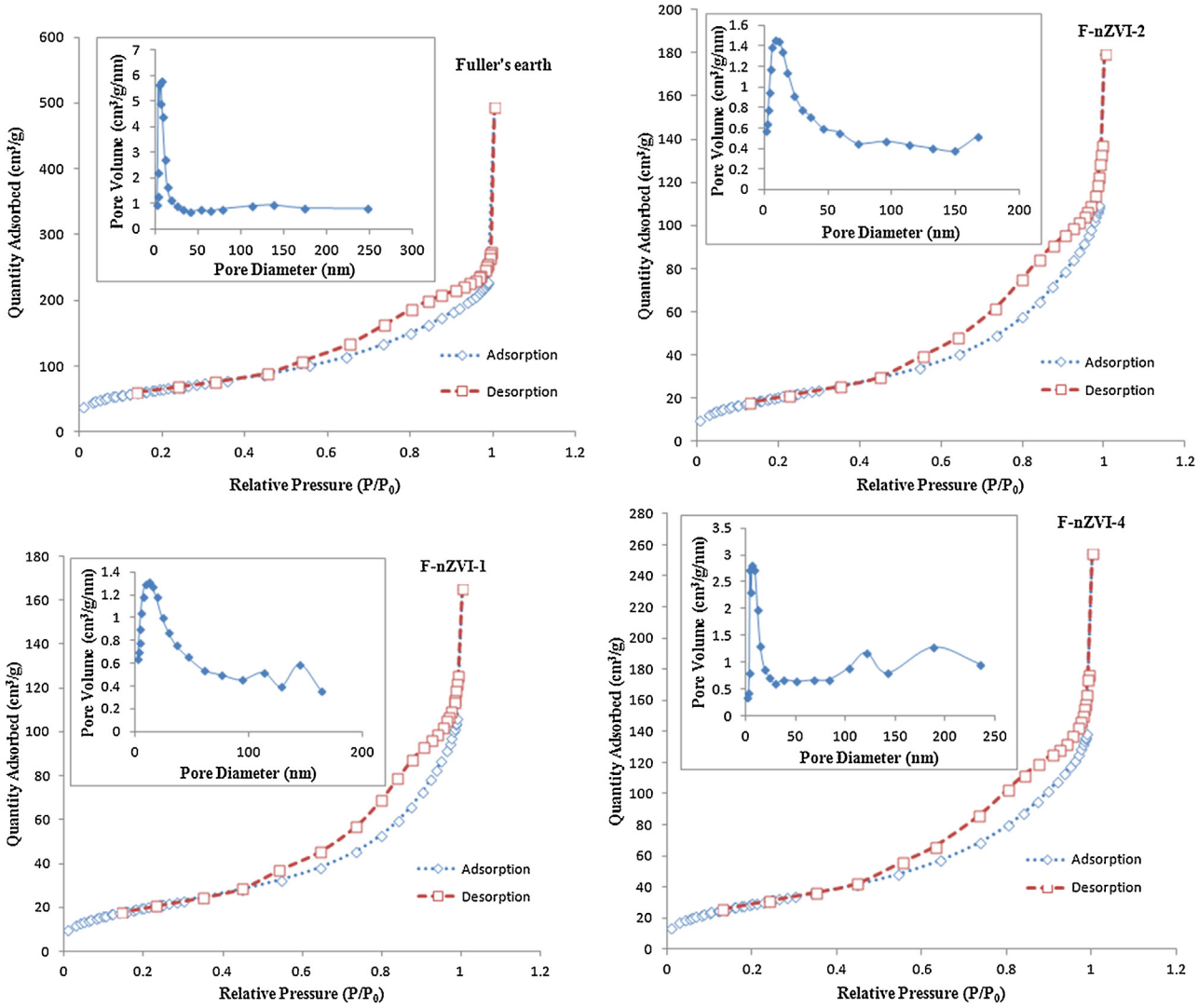

Fig. 5. BET-N_2 adsorption–desorption isotherms and BJH pore size distribution of fuller's earth and F-nZVI 1, 2 and 4.

Table 1
BET-N_2 analysis of fuller's earth and F-nZVI.

Sample	Experimental S_{BET} (m^2/g)	Calculated S_{BET} (m^2/g)	V_{pore} (cm^3/g)	d_{BJH} (nm)
Fuller's earth	230	230	0.371	6.7
F-nZVI-1	73.54	218.84	0.168	8.1
F-nZVI-2	75.47	213.93	0.172	8.4
F-nZVI-4	108.17	185.38	0.220	7.7

arsenic adsorption on F-nZVI. Thus, the hydroxyl moiety is key to higher As(V) adsorption in comparison to As(III) on F-nZVI. The changes in the absorption band corresponding to hydroxyl moiety of F-nZVI in presence of As(III) and As(V) could be accounted to the change in surface of nZVI leading to reduced interaction of hydroxyl moiety with Fe surface during the redox adsorption. A significant change due to narrowing of band at 1047 and 1046 cm^{-1} were observed, upon adsorption of As(III) and As(V) onto the surface of F-nZVI-4. In this case, arsenic adsorption on the surface of F-nZVI probably resulted in the conversion of Fe^0 to Fe(III)/Fe(II) due to weakening of bond between fuller's earth and nZVI. Thus, these results suggest the adsorption of As(III) and As(V) onto the surface of F-nZVI, by an interaction between nZVI and oxoanion.

3.2.4. XRD

The XRD pattern of fuller's earth, F-nZVI-4, As(III) and As(V) adsorbed F-nZVI-4 is given in Fig. 7. The major peak in the XRD pattern of fuller's earth appeared at 2θ of 26.62°, characteristic of quartz and 25.34° corresponding to TiO_2 (Fig. 7a). The peak appearing at 2θ of 35.15° is characteristics of montmorillonite [60]. The 2θ peaks corresponding to Al_2O_3 were observed at 37.11° and 42.41°, while those for Fe_2O_3 were realized at 2θ peak of 19.84° [61]. However, the XRD pattern of F-nZVI-4 retained the peaks corresponding to quartz, Fe_2O_3 and montmorillonite (Fig. 7b). Further the diffraction peaks at 2θ of 44.9° as shown in Fig. 7b, corresponds to the existence of iron in its zerovalent (Fe^0) state [62]. This indicates that Fe^0 nanoparticles were immobilized on the fuller's earth surface. The XRD pattern of F-nZVI-4 showed

significant change upon adsorption of As(III) and As(V) as depicted in Fig. 7c and d, respectively. The peak corresponding to nZVI disappeared and new peaks were observed at 2θ of 35.70°, 57.2° and 62.50°, for the oxide in the form of $Fe_3O_4/\gamma\text{-}Fe_2O_3$ [63]. This accounts for the oxidation of Fe^0 to iron oxide in presence of As(III) and As(V), with the shell of Fe—OH formed on the surface of F-nZVI-4. Thus, it could be concluded that the surface of fuller's earth offers more stability, which is consistent with the results obtain for nZVI immobilized on similar materials like bentonite [64], kaolinite [65], and zeolite [48]. Moreover, there were no diffraction pattern characteristic of precipitation of iron arsenite/iron arsenate observed in case of As(III) and As(V) adsorbed F-nZVI, as evident in ZVI [66]. The ZVI (iron filings) get oxidized on the surface releasing Fe(II) ions in the solution, which co-precipitates as $Fe_3(AsO_4)_2$. Similar phenomenon were observed by Li et al. in case of nZVI upon prolonged exposure (5 days) with As(V) in the solution, which indicates that the oxidation of Fe^0 is complete upon prolonged stay which further leads to the co-precipitation [67]. This suggests that the Fe^0 on the surface is oxidized and electron transfer ceased from the bulk in case of ZVI or completely aged nZVI, which leads to the co-precipitation, which requires detailed independent investigation. Thus, the results of our study corroborate with the reduction–oxidation based adsorption As(III) and As(V) ions with no co-precipitation involved in the sorption phenomenon. The mechanism involves the surface passivation of nZVI with As, which does not interfere with the electron flow between the core and shell of partially oxidized nZVI in succeeding redox adsorption [66,68].

3.2.5. TGA

The TGA analysis for fuller's earth and F-nZVI-4 were carried out in air as depicted in Fig. 8. The fuller's earth exhibits a smooth TGA curve with a weight loss of upto 15% in the temperature range of 25–150 °C. On the other hand, the TGA curve of F-nZVI-4 showed a weight loss of 6% upto 100 °C. The weight loss of F-nZVI-4 is approximately stable in the temperature range 100–280 °C and rapidly for 280–360 °C weight loss was observed upto 9%, followed by a weight gain upto 3% at 450 °C. The weight loss at 100 °C is assigned to water and methanol desorption [69]. The rapid decrease in the weight at 280–360 °C could be accounted to the capillary forces holding micropore water, which are strongly held in the lattice of aluminosilicates of the adsorbent [70]. However, the presence of PEG on the surface of F-nZVI-4 cannot be overruled. The weight gain at 450 °C could be attributed to the thermal oxidation of Fe^0 in air which furnishes Fe_2O_3 which leads to increases in the weight of the material [47].

3.3. Adsorption studies

3.3.1. Effect of pH

The As(III) and As(V) in water exists in many protonated forms, which altogether show different adsorption behaviour. Thus, pH of the arsenic solution plays a crucial role in adsorption. Arsenic adsorptions by F-nZVI were carried out at different pH in the range 3–10. Upon increasing the pH of solution from 3 upto 10, a decrease in As(V) adsorption from 40% at pH 3 to 20% at pH 10 was observed (Fig. 9). Similarly, the effect of pH on As(III) adsorption showed an increase in adsorption upon increasing pH from 3 to 8 with an increase in adsorption from <5 to 25%, at pH 8. Further increase in the pH of solution up to 10, a significant lowering of the adsorption up to 20% of As(III) was observed. Thus, As(III) and As(V) removal efficiency of F-nZVI was optimum at pH 8 and 3, respectively. Further pH increase or decrease from optimum value, the adsorption of As(III) and As(V) decreased sharply.

Similar behaviour of nZVI and immobilized nZVI for adsorption of As(V) and As(III) have been reported under acidic and neutral conditions, respectively. The protonation behaviour of As(III), As(V) and F-nZVI play a significant role in As(III) and As(V) adsorption. The dissociation constant for the stepwise deprotonation of arsenate and arsenite species in aqueous conditions is depicted as:

			pK	As(III)	As(V)
H_3A	⇌	$H_2A^- + H^+$	pKa_1	9.23	2.22
H_2A^-	⇌	$HA^{2-} + H^+$	pKa_2	12.1	6.98
HA^-	⇌	$A^{3-} + H^+$	pKa_3	12.7	11.53

Arsenate exists in the dibasic and monobasic forms in pH range 2–7 and 7–11, respectively, whereas, arsenite exists in the neutral form in the pH range of 2–9. The surface of nZVI based materials are positively charged in the presence of protons [71,72], leading to an electrostatic interaction between dibasic arsenate ($H_2AsO_4^-$) and F-nZVI. However, with increase in the pH there is a decrease in the surface protonation, hence lowered electrostatic interaction is observed between As(V) and immobilized nZVI. Alternatively, H^+ ions are essential for the redox based adsorption of As(V) on to F-nZVI [73]. Thus, the arsenate adsorption decreases with increase in the pH of the solution. However, in case of arsenite adsorption by F-nZVI, the interaction between the positive surface of immobilized nZVI and neutral arsenite is unfavourable [72]. However at pH 8, there is an optimized adsorption for As(III) due to the favourable interaction between the near neutral nZVI and neutral arsenite in the solution. At pH above 9, the concentration of H^+ ions is significantly diminished for favourable reductive adsorptions of arsenite [74]. Alternatively, under alkaline conditions the interaction between the negatively charged arsenite ($H_2AsO_3^-$) and negatively charged corrosion surface products of nZVI are unfavourable [72,75]. Thus, the adsorption of arsenite by F-nZVI is observed at pH 8 [71,72].

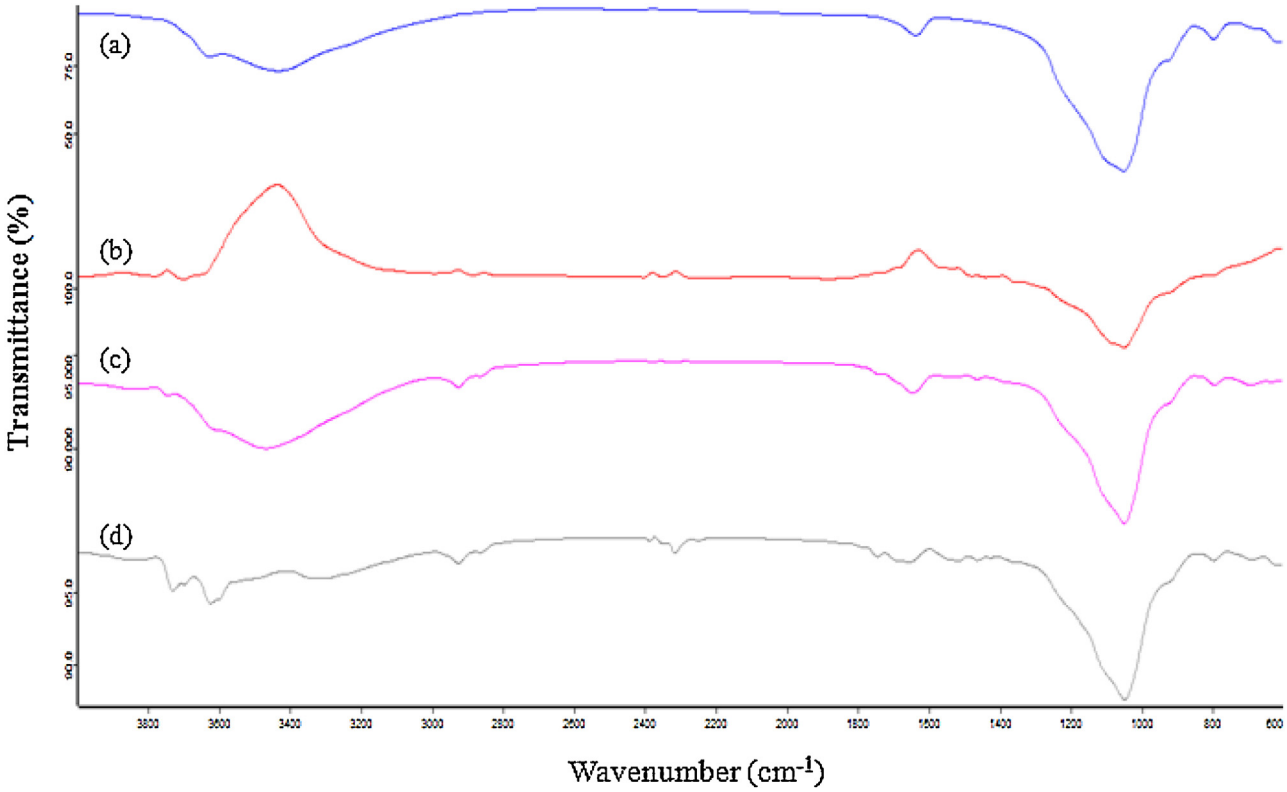

Fig. 6. FTIR spectra of (a) fuller's earth; (b) F-nZVI-4; (c) As(III) adsorbed F-nZVI-4 and (d) As(V) adsorbed F-nZVI-4.

3.3.2. Effect of initial arsenic concentration

The effect of initial As(III) and As(V) concentration on removal efficiency of F-nZVI-4 was investigated in the concentration range of 20–100 mg/L at pH 7 and 3, respectively (Fig. 10). At lower concentration the percentage removal of both As(III) and As(V) were higher. However, with increase in concentration of As(III) and As(V), the removal efficiency of F-nZVI decreased. Increase in concentration of As(III)/As(V) for the same amount of adsorbent may be the reason for the decrease in removal efficiency [76].

3.3.3. Effect of absorbent (F-nZVI) dose

The effect of adsorbent dose on As(III) and As(V) removal was studied by varying the adsorbent dose from 0.2 to 1 g/L, at 10 mg/L of As(III) and As(V) concentration (Fig. 11). The result showed an increase in As(III) and As(V) removal from 13.85 to 45.23% and 17.20 to 76.86%, respectively, with an increase of F-nZVI dose from 0.2 to 1 g/L.

Increase in removal of As(III) and As(V) by F-nZVI-4, is accounted to the increase in surface area and number of adsorption sites with the increase in adsorbent dose [77,78]. On the other hand, a decrease in the arsenic uptake (q_e) was observed with an increase of F-nZVI dose. The decrease in arsenic uptake (q_e) is accounted to the availability of lesser number of As(III) and As(V) per unit mass of the F-nZVI, due to which the active sites may remain unsaturated during the adsorption process [76].

3.3.4. Effect of contact time and kinetics behaviour

The effect of contact time on As(III) and As(V) removal by F-nZVI was studied by varying the contact time upto 24 h, with adsorbent dose of 1 g/L, initial arsenic concentration of 100 mg/L maintained at optimum pH of 8 and 3 for As(III) and As(V), respectively. As shown in Fig. 12, the efficiency of F-nZVI for As(III) and As(V) removal increased significantly with increased time period of contact with the adsorbent and equilibrium was achieved at 10 h. The plot between As(III) and As(V) removal and time (Fig. 12) indicate faster rate of arsenic adsorption in the initial stage which subsequently decreased after 8 h till the attainment of equilibrium. The As(III) and As(V) removal upto 40.29 and 54.76%, respectively were observed in first 6 h of addition of F-nZVI. When contact time was increased from 6 to 10 h, the removal of As(III) and As(V) subsequently increased from 40.29 and 54.76% to 49.39 and 62.12%, respectively.

The time dependent variation in equilibrium concentration of As(III) and As(V) were fitted to pseudo-first order and pseudo-second order rate kinetic model. The pseudo-first order (Eq. (2)) and pseudo-second order (Eq. (3)) rate equation are as described below:

$$\log(q_e - q_t) = \log(q_e) - k_1 t \tag{2}$$

$$\frac{t}{q_t} = k_2 {q_e}^2 + \frac{1}{q_e \times t} \tag{3}$$

where q_e and q_t are the amount of As(III) and As(V) adsorbed (mg/g) at equilibrium and at time t (h), respectively. k_1 and k_2 is the rate constant of the pseudo-first order and pseudo-second order adsorption rate (g/mg/h), respectively. The data were best fitted into pseudo-second order rate kinetics model. Pseudo-first order kinetic model showed poor fitting for the data and were not considered.

The values of k_2 and q_e were calculated from the slope and intercept of the plot t/q_t vs. t, for both As(III) and As(V) as given in Fig. 13. The kinetics parameters k_2,q_e and R^2 of F-nZVI 1, 2, 3, 4 and 8 for adsorption of As(III) and As(V) are listed in Table 2. The positive value of k_2 and q_e suggest that the overall rate of arsenic adsorption onto F-nZVI was controlled by pseudo-second order reaction mechanism. The results indicate an increase in the rate constant for the pseudo-second order conditions, upon increasing

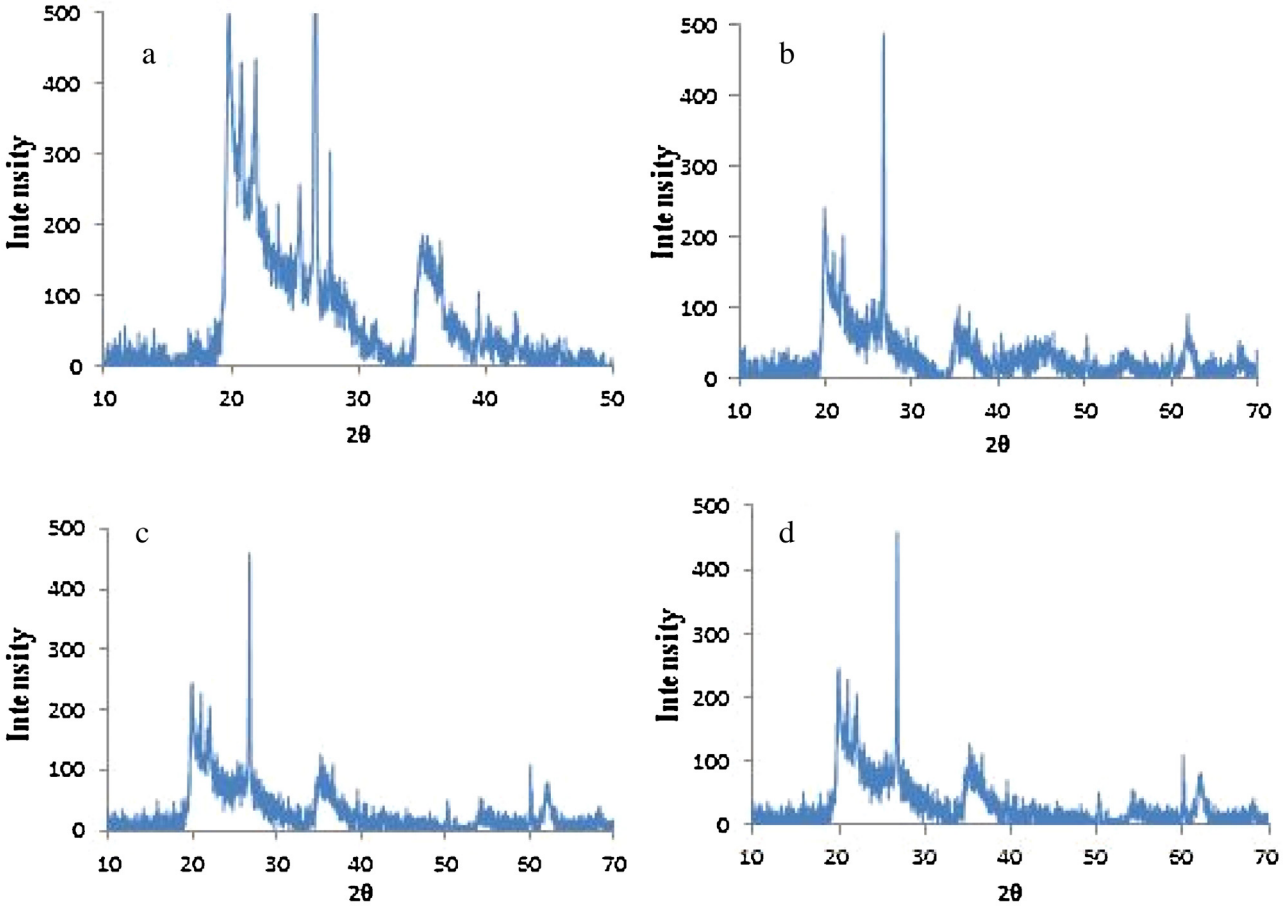

Fig. 7. X-ray diffraction patterns of (a) fuller's earth, (b) F-nZVI-4, (c) and (d) F-nZVI-4 after adsorption of As(III) and As(V).

the loading of F-nZVI upto 20% (w/w). This increase in k_2 could be accounted to the increase in the surface area of F-nZVI due to reduced agglomeration, which resulted in increased interaction with arsenic in aqueous solution. However, there was a significant fall in k_2 in case of F-nZVI-8, in comparison to F-nZVI 1-4 for adsorption of As(V), which could be accounted to the decrease in the surface area of immobilized nZVI, due to aggregation on fuller's earth surface. Thus, it could be concluded that fast kinetics of adsorption is achieved at 20% (w/w) nZVI loading on fuller's earth. Various studies suggest that initially diffusion occurs by external mass transfer followed by intraparticle diffusion occurs incase of arsenic adsorption by nZVI [79,80]. Initially, there is a large concentration gradient between the solution and the adsorbent surface leading to a faster transfer of adsorbate onto the adsorbent surface. However, with the passage of time, predominantly intraparticle diffusion of adsorbate from surface of adsorbent to internal adsorption sites of adsorbent occurs, by a slow process [76]. Thus based on the above phenomenon, the reductive sorption of arsenic using nZVI [81,82], is proposed to take place in three steps involving: (i) the diffusion of the solute from the bulk solution of the As(III) and As(V) to the exterior surface of the adsorbent; (ii) intraparticle diffusion to the interior of the nZVI and

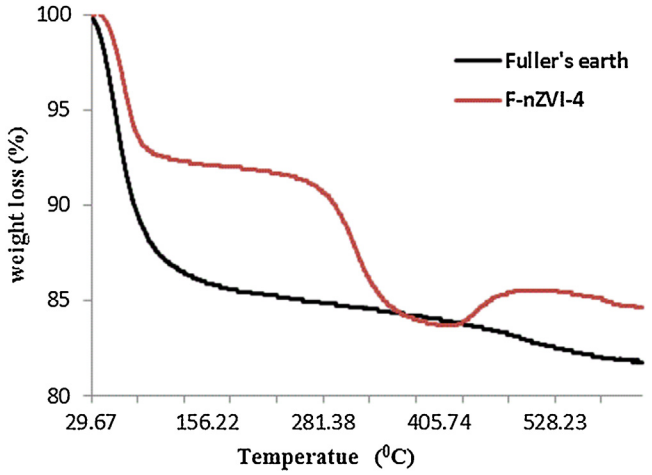

Fig. 8. TGA curve of fuller's earth and F-nZVI-4.

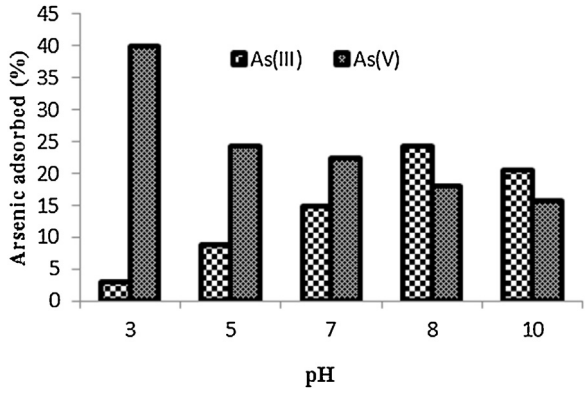

Fig. 9. Effect of pH on adsorption of As(III) and As(V) by F-nZVI-4, [As] = 50 mg/L, 25 °C and 150 rpm.

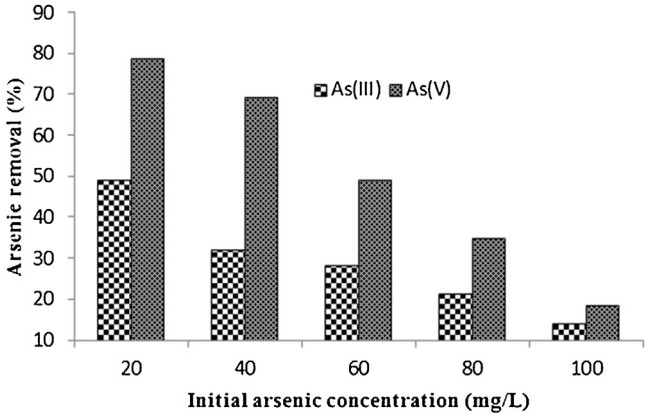

Fig. 10. Effect of initial arsenic concentration on F-nZVI [F-nZVI 1 g/L, As-20-100 mg/L, pH 8 and 3 at 25 °C and 150 rpm for As(III) and As(V), respectively].

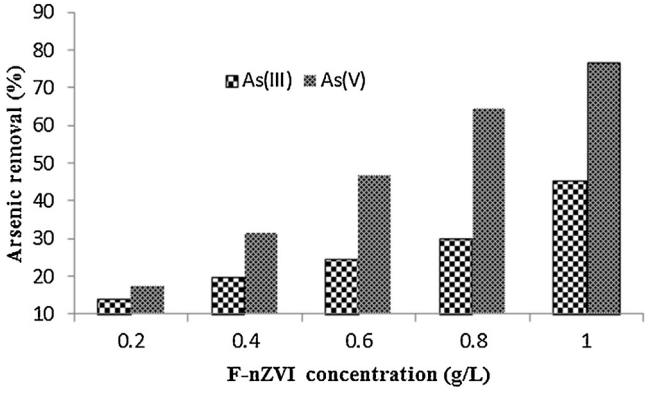

Fig. 11. Effect of F-nZVI dose on the As(III) and As(V) remediation, [As] = 10 mg/L at pH 8 and 3, respectively, 25 °C 150 rpm.

(iii) adsorption in the inner site of the nZVI. Therefore, As(III)/As(V) in the aqueous solution is initially adsorbed onto the iron oxide shell of F-nZVI. Upon saturation of the exterior surface, arsenic diffuses through the iron oxide shell and adsorbed to the interior surface. Further, the kinetics of As(III) adsorption on F-nZVI was found to be slower than As(V) adsorption could be accounted to the

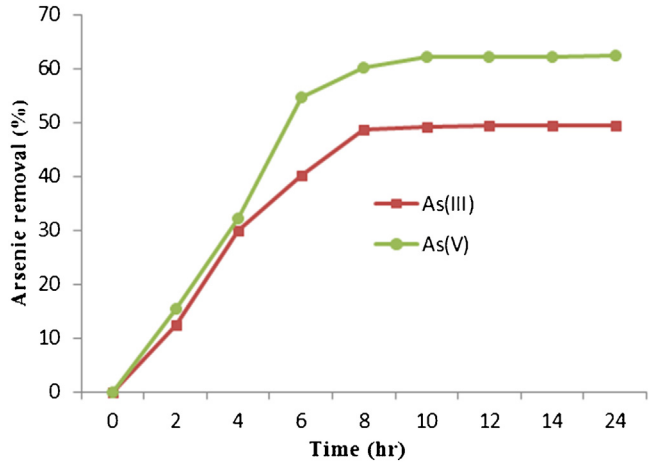

Fig. 12. Effect of contact time on As(III) and As(V), [As] = 100 mg/L at pH 8, 25 °C, 150 rpm.

diffusion of adsorbate from solution to the surface oxide shell being fast incase of As(V) in comparison to As(III). However, the lower proton concentration in case of As(III) adsorption in comparison to As(V) adsorption may also contribute significantly to the slow adsorption of As(III).

3.4. Equilibrium adsorption studies

The equilibrium adsorption studies were carried out to reveal the adsorption of As(III) and As(V) on F-nZVI 1–8, as depicted in Fig. 14. Different concentration (20–100 mg/L) of As(III) and As(V) were treated with optimum adsorbent dose (1 g/L) at pH 8 and 3, respectively, for 24 h. The F-nZVI showed an increase in the adsorption of both As(III) and As(V), upon increasing the iron loading from 5 to 20% (*w/w*). However, further increase in the iron loading from 25 to 50% (w/w) on fuller's earth, showed insignificant adsorption of both As(III) and As(V) from aqueous solution. These results showed that the F-nZVI 1–4 with lower iron loading were stabilized on fuller's earth surface and did not agglomerate, which increased the active surface area of these F-nZVI. However, F-nZVI 5–8 showed a decrease in the adsorption of arsenic with increase in the loading of iron, resulting in agglomeration of the nanoparticles on the surface of fuller's earth

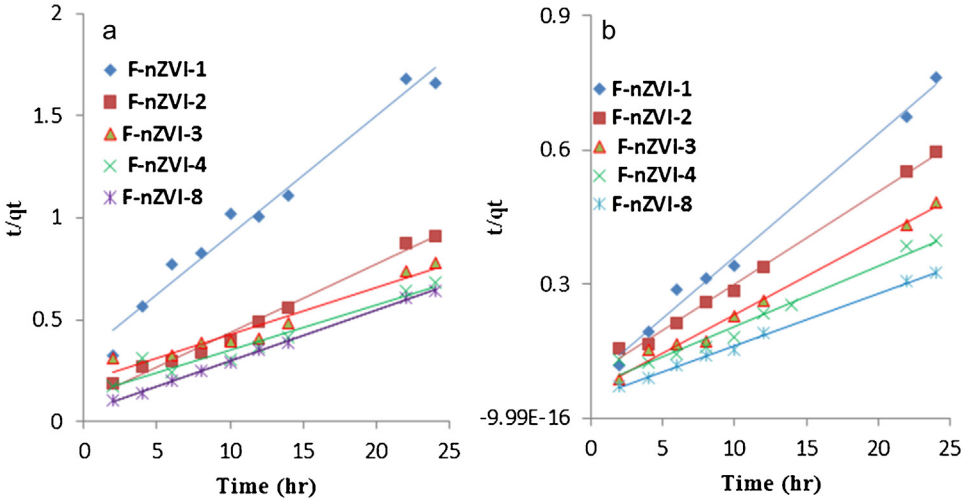

Fig. 13. Pseudo-second order kinetics of F-nZVI for (a) As(III) at pH 8; and (b) As(V) at pH 3, [As] = 50 mg/L at 25 °C, 150 rpm.

Table 2
Pseudo-second order rate constant for As(III) and As(V) adsorption on F-nZVI [As] = 10 mg/L, 25 °C, 150 rpm maintained at pH 8 and 3.

F-nZVI	Pseudo-second order kinetics					
	Arsenite			Arsenate		
	k_2 (g mg^{-1} h^{-1})	q_e (mg/g)	R^2	k_2 (g mg^{-1} h^{-1})	q_e (mg/g)	R^2
1	0.492	17.24	0.972	3.33	37.03	0.991
2	1.55	30.30	0.990	4.39	50.00	0.991
3	2.67	43.74	0.939	8.08	58.82	0.989
4	3.20	45.45	0.937	8.87	76.92	0.971
8	3.01	41.64	0.998	1.26	90.90	0.997

as evident from the SEM imaging. Apart from this, F-nZVI-4 showed maximum adsorption for both As(III) and As(V) in comparison to other F-nZVI, which established an optimized condition for iron loading of fuller's earth with maximum activity.

The adsorption isotherm for As(III) and As(V) adsorption upon F-nZVI 1–8 were analysed by non-linear Langmuir and Freundlich adsorption isotherm model (Fig. 15). These isotherm equations were used to quantitatively describe the effect of increased aqueous arsenic concentration on the F-nZVI surface. The Langmuir isotherm represents monolayer adsorption whereby surface contains a finite number of identical sites for adsorption. The model assumes uniform energies for adsorption onto the surface and no transmigration of adsorbate in the plane of the surface.

The equation for non-linear Langmuir isotherm is represented as:

$$q_e = \frac{q_m K_L C_e}{1 + K_L C_e}$$

where C_e is the equilibrium concentration of adsorbate (mg/L), q_e is the amount of metal adsorbed per gram of the adsorbent at equilibrium (mg/g), q_m is maximum monolayer coverage capacity (mg/g) and K_L is Langmuir isotherm constant (L/g) related to the energy of adsorption.

Freundlich isotherm is empirical in nature and describes multilayer adsorption. The equation for non-linear Freundlich isotherm is represented as:

$$q_e = K_F (C_e)^{1/n} \quad (5)$$

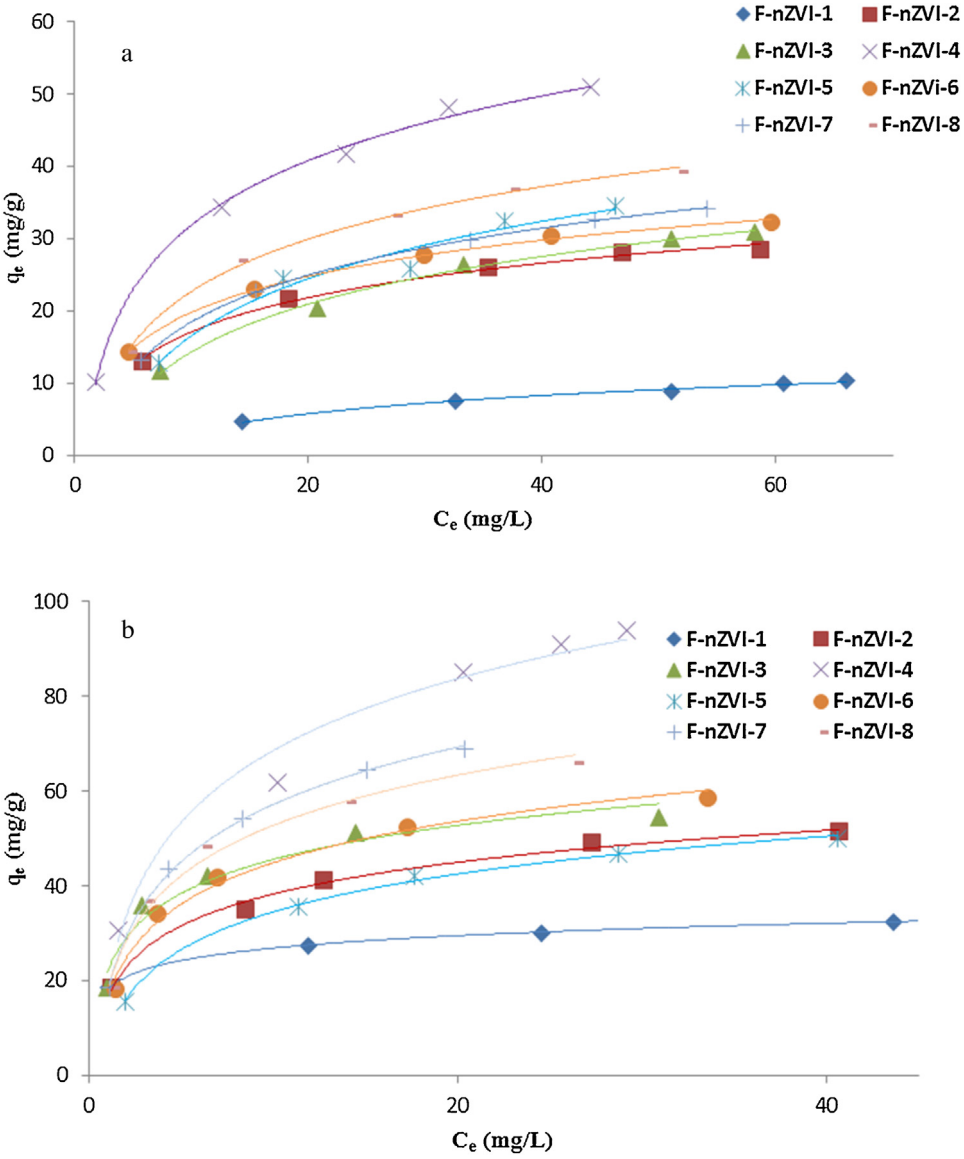

Fig. 14. Adsorption behaviour (a) As(III), and (b) As(V) adsorption on F-nZVI at pH 8 and 3, respectively upon stirring for 24 h at 150 rpm and 25 ± 2 °C.

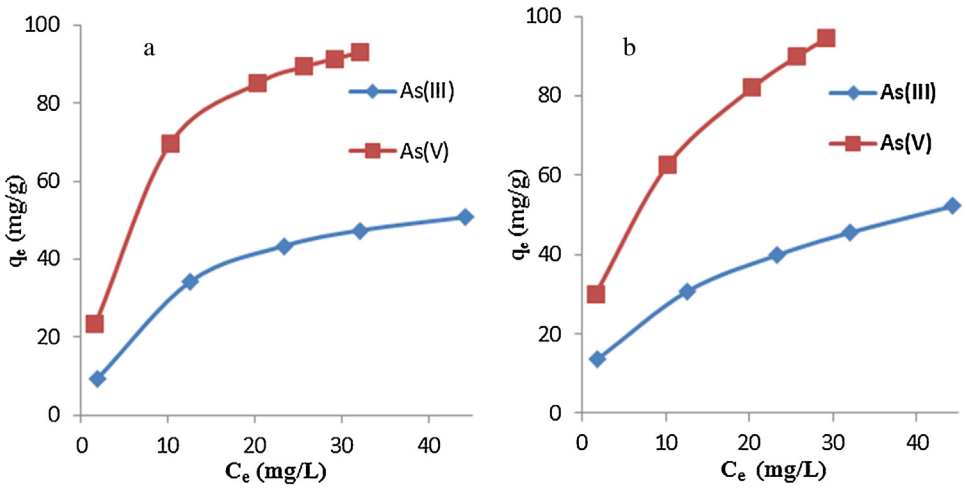

Fig. 15. (a) Langmuir and (b) Freundlich adsorption isotherm for As(III) and As(V) on F-nZVI-4.

Table 3
Adsorption isotherm for As(III) and As(V) adsorption on F-nZVI.

F-nZVI	Arsenite						Arsenate					
	Langmuir			Freundlich			Langmuir			Freundlich		
	q_{max}	K_L	R^2	$1/n$	K_f	R^2	q_{max}	K_L	R^2	$1/n$	K_f	R^2
1	15.42	0.02	0.99	0.73	0.57	0.96	32.13	1.16	0.86	0.14	18.62	0.99
2	33.03	0.10	0.99	0.37	6.64	0.92	53.54	0.30	0.93	0.27	19.92	0.97
3	41.84	0.04	0.99	0.52	4.01	0.92	57.62	0.50	0.98	0.24	25.00	0.86
4	50.80	0.04	0.95	0.42	10.6	0.96	91.42	0.16	0.94	0.39	25.10	0.99
5	49.54	0.05	0.99	0.58	3.64	0.92	56.32	0.16	0.98	0.34	14.71	0.95
6	35.84	0.12	0.98	0.35	8.67	0.92	63.74	0.28	0.99	0.29	21.53	0.91
7	42.06	0.07	0.99	0.42	6.60	0.95	81.18	0.25	0.99	0.38	22.86	0.94
8	47.26	0.09	0.99	0.45	7.01	0.98	73.40	0.29	0.99	0.32	23.73	0.90

where K_F and n are the Freundlich constant related to the adsorption capacity and adsorption intensity, respectively.

The adsorption data fitted well with both Langmuir and Freundlich isotherm models. The constants evaluated from the isotherms are given in Table 3. Adequate linear correlation was observed for both Langmuir and Freundlich isotherm models. The adsorption capacity (q_{max}) of F-nZVI-4 for As(III) and As(V) were found to be 50.08 mg/g and 91.42 mg/g, respectively. The process of adsorption is considered appreciable and indicative of surface adsorption, if the value of $1/n$ is in the range of 0–1. The $1/n$ value for As(III) and As(V) adsorption on F-nZVI 1–8 were found to lie between 0 and 1. As the $1/n$ value lies between 0 and 1, it indicates spontaneous adsorption of As(III)/As(V) on to F-nZVI, irrespective of the iron loading characteristics on the immobilizer. The relevance of the Langmuir isotherm is studied by the Langmuir isotherm constant (K_L). The K_L value of As(III) and As(V) adsorption on F-nZVI were found to lie in the range 0.35–0.73 and 0.14–0.39, respectively. This value of K_L indicates favourable adsorption of As (III) and As(V) on F-nZVI 1–8.

A comparison of the removal efficiency of immobilized iron with different studies on arsenic removal by various iron based material is illustrated in Table 4. Iron filing in sand were studied for arsenic remediation in column filtration, the observed arsenic remediation were sufficient for groundwater conditions [66,84,85]. However, in this method the arsenic remediation was observed to show the formation of iron arsenite precipitates

Table 4
Arsenic removal efficiency of the adsorbents.

S. No.	Material	pH	As(III) (mg/g)	As(V) (mg/g)	References
1	Iron oxide	5	6.77	7.23	[83]
2	Iron filing and sand	7.1	11	–	[66]
3	Sand and ZVI	7	25	–	[84]
4	Sand and ZVI	7	4.4	–	[85]
5	nZVI	6	–	239	[67]
6	Bare nZVI	7	55	17	[86]
7	Cellulose and nZVI	8	19.93	–	[87]
8	Activated char and nZVI	6.5	18.2	12	[88]
9	Montmorillonite–40% nZVI	7	59.9	45.5	[89]
10	Montmorillonite–50% nZVI	6.5	49.5	–	[59]
11	F-nZVI-4	7/3	50.08	91.42	Present study
12	F-nZVI-7	7/3	42.06	81.18	Present study
13	F-nZVI-8	7/3	47.26	73.40	Present study

on the surface as the possible mechanism for the adsorption of arsenic. Bare nZVI alternatively showed better adsorption for As (III) and As(V), whereby the mechanism, suggests the simultaneous reduction and oxidation of arsenic in conjunction with iron oxidation [67]. Li et al. recently reported an adsorption upto 239 mg/g using bare nZVI, in case of smelting wastewater remediation in a pilot scale batch process [67]. The treatment period was upto 5 days and showed a significant amount of $Fe_3(AsO_4)_2$ co-precipitates. Thus, it is envisaged that a detailed work on the ageing of the nZVI based material and its implication on the arsenic adsorption mechanism is required to be studied in greater details.

A comparison with immobilized nZVI such as cellulose [87] and activated char [88] immobilized nZVI, a significant increase in the arsenic adsorption was observed over bare nZVI, however arsenic adsorption is lower than that incase of montmorillonite [59,89] or the fuller's earth immobilized nZVI. The characteristic adsorption incase of montmorillonite was found to be similar to that of the present study under comparable iron loading conditions (40 and 50% w/w Fe^0). However, the present study shows that the iron loading is a crucial factor whereby arsenic adsorption increased upto 20% incase of fuller's earth immobilized nZVI with better rate of adsorption for both As(V) and As(III) using this material. Thus, a better material could be obtained in the present study for arsenic remediation using 60% lesser iron loading in comparison to the previous studies on montmorillonite loaded nZVI.

4. Conclusions

Batch adsorption studies showed that F-nZVI were effective in remediation of both As(III) and As(V) followed pseudo-second order kinetics with higher rate constant for As(V) than As(III). The loading of iron on fuller's earth plays a vital role in the adsorbents activity towards arsenic adsorption. Hence, fuller's earth is a stable, low cost clay mineral and useful support material for n-ZVI, which can be used for remediation of heavy metals.

Acknowledgements

This work was supported in terms of funds, fellowship and Central Instrumentation Facilty by Central University of Punjab, Bathinda for M Phil-PhD work of Mr. Radheshyam Yadav. J. Nagendra Babu is thankful to DST, New Delhi for providing funds through DST Fast Track Young Scientist as Project Ref. No. 240/2010 for research support. We also like to thank the services extended by IIT, Ropar for XRD analysis, and Guru Nanak Dev University for BET analysis.

References

[1] B.K. Mandal, K.T. Suzuki, Arsenic round the world: a review, Talanta 58 (2002) 201–235.
[2] J.M. Neff, Ecotoxicology of arsenic in the marine environment, Environ. Toxicol. Chem. 16 (1997) 917–927.
[3] I. Villaescusa, J.-C. Bollinger, Arsenic in drinking water: sources, occurrence and health effects (a review), Environ. Sci. Biotechnol. 7 (2008) 307–323.
[4] V.K. Sharma, M. Sohn, Aquatic arsenic: toxicity, speciation, transformations, and remediation, Environ. Int. 35 (2009) 743–759.
[5] P. Smedley, D. Kinniburgh, A review of the source, behaviour and distribution of arsenic in natural waters, Appl. Geochem. 17 (2002) 517–568.
[6] N.E. Korte, Q. Fernando, A review of arsenic(III) in groundwater, Crit. Rev. Environ. Sci. Technol. 21 (1991) 1–39.
[7] J. Matschullat, Arsenic in the geosphere—a review, Sci. Total Environ. 249 (2000) 297–312.
[8] W.R. Cullen, K.J. Reimer, Arsenic speciation in the environment, Chem. Rev. 89 (1989) 713–764.
[9] Z. Zhao, Y. Jia, L. Xu, S. Zhao, Adsorption and heterogeneous oxidation of As(III) on ferrihydrite, Water Res. 45 (2011) 6496–6504.
[10] P. Roy, A. Saha, Metabolism and toxicity of arsenic: a human carcinogen, Curr. Sci. 82 (2002) 38–45.
[11] H.M. Bolt, Arsenic: an ancient toxicant of continuous public health impact, from Iceman Ötzi until now, Arch. Toxicol. 86 (2012) 825–830.
[12] S. Kapaj, H. Peterson, K. Liber, P. Bhattacharya, Human health effects from chronic arsenic poisoning—a review, J. Environ. Sci. Health Part A 41 (2006) 2399–2428.
[13] M.I. Litter, M.E. Morgada, J. Bundschuh, Possible treatments for arsenic removal in Latin American waters for human consumption, Environ. Pollut. 158 (2010) 1105–1118.
[14] W. Burgess, M. Hoque, H. Michael, C. Voss, G. Breit, K. Ahmed, Vulnerability of deep groundwater in the Bengal Aquifer System to contamination by arsenic, Nat. Geosci. 3 (2010) 83–87.
[15] A. Oehmen, R. Valerio, J. Llanos, J. Fradinho, S. Serra, M.A. Reis, J.G. Crespo, S. Velizarov, Arsenic removal from drinking water through a hybrid ion exchange membrane–coagulation process, Sep. Purif. Technol. 83 (2011) 137–143.
[16] J. Kim, M.M. Benjamin, Modeling a novel ion exchange process for arsenic and nitrate removal, Water Res. 38 (2004) 2053–2062.
[17] C.-Y. Cao, J. Qu, W.-S. Yan, J.-F. Zhu, Z.-Y. Wu, W.-G. Song, Low-cost synthesis of flowerlike α-Fe_2O_3 nanostructures for heavy metal ion removal: adsorption property and mechanism, Langmuir 28 (2012) 4573–4579.
[18] D.E. Giles, M. Mohapatra, T.B. Issa, S. Anand, P. Singh, Iron and aluminium based adsorption strategies for removing arsenic from water, J. Environ. Manage. 92 (2011) 3011–3022.
[19] S.R. Chowdhury, E.K. Yanful, A.R. Pratt, Arsenic removal from aqueous solutions by mixed magnetite–maghemite nanoparticles, Environ. Earth Sci. 64 (2011) 411–423.
[20] J. Wang, C. Chen, Biosorbents for heavy metals removal and their future, Biotechnol. Adv. 27 (2009) 195–226.
[21] B. Volesky, Detoxification of metal-bearing effluents: biosorption for the next century, Hydrometallurgy 59 (2001) 203–216.
[22] D. Mohan, A. Sarswat, Y.S. Ok, C.U. Pittman, Organic and inorganic contaminants removal from water with biochar, a renewable, low cost and sustainable adsorbent—a critical review, Bioresour. Technol. 160 (2014) 191–202.
[23] R. Kumar, R. Kumar, S. Mittal, M. Arora, J.N. Babu, Role of soil physicochemical characteristics on the present state of arsenic and its adsorption in alluvial soils of two agri-intensive region of Bathinda, Punjab, India, J. Soils Sediments (2015) 1–16.
[24] Y.-h. Xu, T. Nakajima, A. Ohki, Adsorption and removal of arsenic(V) from drinking water by aluminum-loaded Shirasu-zeolite, J. Hazard. Mater. 92 (2002) 275–287.
[25] X.-H. Guan, T. Su, J. Wang, Quantifying effects of pH and surface loading on arsenic adsorption on NanoActive alumina using a speciation-based model, J. Hazard. Mater. 166 (2009) 39–45.
[26] S. Bajpai, M. Chaudhuri, Removal of arsenic from ground water by manganese dioxide-coated sand, J. Environ. Eng. 125 (1999) 782–784.
[27] T. Türk, I. Alp, H. Deveci, Adsorption of As(V) from water using Mg–Fe-based hydrotalcite (FeHT), J. Hazard. Mater. 171 (2009) 665–670.
[28] C. Ardau, C. Cannas, M. Fantauzzi, A. Rossi, L. Fanfani, Arsenic removal from surface waters by hydrotalcite-like sulphate minerals: field evidences from an old mine in Sardinia, Italy, Neues Jahrbuch für Mineralogie-Abhandlungen, J. Mineral. Geochem. 188 (2011) 49–63.
[29] W. Hartley, N.W. Lepp, Remediation of arsenic contaminated soils by iron-oxide application, evaluated in terms of plant productivity, arsenic and phytotoxic metal uptake, Sci. Total Environ. 390 (2008) 35–44.
[30] M.A. Ramos, W. Yan, X.-q. Li, B.E. Koel, W.-x. Zhang, Simultaneous oxidation and reduction of arsenic by zero-valent iron nanoparticles: understanding the significance of the core- shell structure, J. Phys. Chem. C 113 (2009) 14591–14594.
[31] J.-H. Huang, E.J. Elzinga, Y. Brechbuehl, A. Voegelin, R. Kretzschmar, Impacts of Shewanella putrefaciens strain CN-32 cells and extracellular polymeric substances on the sorption of As(V) and As(III) on Fe(III)-(hydr) oxides, Environ. Sci. Technol. 45 (2011) 2804–2810.
[32] J. Bundschuh, M.I. Litter, F. Parvez, G. Román-Ross, H.B. Nicolli, J.-S. Jean, C.-W. Liu, D. Lopez, M.A. Armienta, L.R. Guilherme, One century of arsenic exposure in Latin America: a review of history and occurrence from 14 countries, Sci. Total Environ. 429 (2012) 2–35.
[33] R. Crane, T. Scott, Nanoscale zero-valent iron: future prospects for an emerging water treatment technology, J. Hazard. Mater. 211 (2012) 112–125.
[34] M. Chrysochoou, C.P. Johnston, G. Dahal, A comparative evaluation of hexavalent chromium treatment in contaminated soil by calcium polysulfide and green-tea nanoscale zero-valent iron, J. Hazard. Mater. 201 (2012) 33–42.
[35] F. Liang, J. Fan, Y. Guo, M. Fan, J. Wang, H. Yang, Reduction of nitrite by ultrasound-dispersed nanoscale zero-valent iron particles, Ind. Eng. Chem. Res. 47 (2008) 8550–8554.
[36] H. Kim, H.-J. Hong, J. Jung, S.-H. Kim, J.-W. Yang, Degradation of trichloroethylene (TCE) by nanoscale zero-valent iron (nZVI) immobilized in alginate bead, J. Hazard. Mater. 176 (2010) 1038–1043.
[37] R. Singh, V. Misra, R.P. Singh, Remediation of γ-hexachlorocyclohexane contaminated soil using nanoscale zero-valent iron, J. Bionanosci. 5 (2011) 82–87.
[38] Y. Li, W. Cheng, G. Sheng, J. Li, H. Dong, Y.C.L. Zhu, Synergetic effect of a pillared bentonite support on Se(VI) removal by nanoscale zero valent iron, Appl. Catal. B: Environ. 174 (2015) 329–335.

[39] X. Bai, Z.-F. Ye, Y.-Z. Qu, Y.-F. Li, Z.-Y. Wang, Immobilization of nanoscale Fe^0 in and on PVA microspheres for nitrobenzene reduction, J. Hazard. Mater. 172 (2009) 1357–1364.
[40] F. Fu, J. Ma, L. Xie, B. Tang, W. Han, S. Lin, Chromium removal using resin supported nanoscale zero-valent iron, J. Environ. Manage. 128 (2013) 822–827.
[41] X. Lv, J. Xu, G. Jiang, X. Xu, Removal of chromium(VI) from wastewater by nanoscale zero-valent iron particles supported on multiwalled carbon nanotubes, Chemosphere 85 (2011) 1204–1209.
[42] A.K. Sharma, R. Kumar, S. Mittal, S. Hussain, M. Arora, R.C. Sharma, J.N. Babu, In situ reductive regeneration of zerovalent iron nanoparticles immobilized on cellulose for atom efficient Cr(vi) adsorption, RSC Adv. 5 (2015) 89441–89446.
[43] A.N. Bezbaruah, H. Kalita, T. Almeelbi, C.L. Capecchi, D.L. Jacob, A.G. Ugrinov, S. A. Payne, Ca–alginate-entrapped nanoscale iron: arsenic treatability and mechanism studies, J. Nanopart. Res. 16 (2014) 1–10.
[44] T. Liu, Z.-L. Wang, L. Zhao, X. Yang, Enhanced chitosan/Fe^0-nanoparticles beads for hexavalent chromium removal from wastewater, Chem. Eng. J. 189 (2012) 196–202.
[45] L. Wu, L. Liao, G. Lv, F. Qin, Y. He, X. Wang, Micro-electrolysis of Cr(VI) in the nanoscale zero-valent iron loaded activated carbon, J. Hazard. Mater. 254 (2013) 277–283.
[46] L. Yang, L. Lv, S. Zhang, B. Pan, W. Zhang, Catalytic dechlorination of monochlorobenzene by Pd/Fe nanoparticles immobilized within a polymeric anion exchanger, Chem. Eng. J. 178 (2011) 161–167.
[47] E. Petala, K. Dimos, A. Douvalis, T. Bakas, J. Tucek, R. Zbořil, M.A. Karakassides, Nanoscale zero-valent iron supported on mesoporous silica: characterization and reactivity for Cr(VI) removal from aqueous solution, J. Hazard. Mater. 261 (2013) 295–306.
[48] S.A. Kim, S. Kamala-Kannan, K.-J. Lee, Y.-J. Park, P.J. Shea, W.-H. Lee, H.-M. Kim, B.-T. Oh, Removal of Pb(II) from aqueous solution by a zeolite–nanoscale zero-valent iron composite, Chem. Eng. J. 217 (2013) 54–60.
[49] Z. Pang, M. Yan, X. Jia, Z. Wang, J. Chen, Debromination of decabromodiphenyl ether by organo-montmorillonite-supported nanoscale zero-valent iron: preparation, characterization and influence factors, J. Environ. Sci. 26 (2014) 483–491.
[50] X. Zhang, S. Lin, Z. Chen, M. Megharaj, R. Naidu, Kaolinite-supported nanoscale zero-valent iron for removal of Pb^{2+} from aqueous solution: reactivity, characterization and mechanism, Water Res. 45 (2011) 3481–3488.
[51] Y. Li, J. Li, Y. Zhang, Mechanism insights into enhanced Cr(VI) removal using nanoscale zerovalent iron supported on the pillared bentonite by macroscopic and spectroscopic studies, J. Hazard. Mater. 227 (2012) 211–218.
[52] N. Horzum, M.M. Demir, M. Nairat, T. Shahwan, Chitosan fiber-supported zero-valent iron nanoparticles as a novel sorbent for sequestration of inorganic arsenic, RSC Adv. 3 (2013) 7828–7837.
[53] G. Atun, G. Hisarli, W. Sheldrick, M. Muhler, Adsorptive removal of methylene blue from colored effluents on fuller's earth, J. Colloid Interface Sci. 261 (2003) 32–39.
[54] J.U.K. Oubagaranadin, N. Sathyamurthy, Z. Murthy, Evaluation of fuller's earth for the adsorption of mercury from aqueous solutions: a comparative study with activated carbon, J. Hazard. Mater. 142 (2007) 165–174.
[55] G.-m. Cao, M. Sheng, W.-f. Niu, Y.-l. Fei, D. Li, Regeneration and reuse of iron catalyst for Fenton-like reactions, J. Hazard. Mater. 172 (2009) 1446–1449.
[56] D.V. Kerkez, D.D. Tomašević, G. Kozma, M.R. Bečelić-Tomin, M.D. Prica, S.D. Rončević, Á. Kukovecz, B.D. Dalmacija, Z. Kónya, Three different clay-supported nanoscale zero-valent iron materials for industrial azo dye degradation: a comparative study, J. Taiwan Inst. Chem. Eng. 45 (2014) 2451–2461.
[57] L. Tang, J. Tang, G. Zeng, G. Yang, X. Xie, Y. Zhou, Y. Pang, Y. Fang, J. Wang, W. Xiong, Rapid reductive degradation of aqueous *p*-nitrophenol using nanoscale zero-valent iron particles immobilized on mesoporous silica with enhanced antioxidation effect, Appl. Surf. Sci. 333 (2015) 220–228.
[58] K. Bukka, J. Miller, J. Shabtai, FTIR study of deuterated montmorillonites: structural features relevant to pillared clay stability, Clays Clay Miner. 40 (1992) 92–102.
[59] P.K. Tandon, R.C. Shukla, S.B. Singh, Removal of arsenic(III) from water with clay-supported zerovalent iron nanoparticles synthesized with the help of tea liquor, Ind. Eng. Chem. Res. 52 (2013) 10052–10058.
[60] J. Xu, Y. Li, C. Jing, H. Zhang, Y. Ning, Removal of uranium from aqueous solution using montmorillonite-supported nanoscale zero-valent iron, J. Radioanal. Nucl. Chem. 299 (2014) 329–336.
[61] Y. Subbareddy, C. Jayakumar, S. Valliammai, K. Nagaraja, B. Jeyaraj, Equilibrium, kinetic and thermodynamic study of adsorption of rhodamine B dye from aqueous solution by fuller's earth, Inte. J. Res. Chem. Environ. 4 (2014) 16–25.
[62] K. Sohn, S.W. Kang, S. Ahn, M. Woo, S.-K. Yang, Fe(0) nanoparticles for nitrate reduction: stability, reactivity, and transformation, Environ. Sci. Technol. 40 (2006) 5514–5519.
[63] X. Lv, J. Xu, G. Jiang, J. Tang, X. Xu, Highly active nanoscale zero-valent iron (nZVI)–Fe 3 O 4 nanocomposites for the removal of chromium(VI) from aqueous solutions, J. Colloid Interface Sci. 369 (2012) 460–469.
[64] L.-n. Shi, X. Zhang, Z.-l. Chen, Removal of chromium(VI) from wastewater using bentonite-supported nanoscale zero-valent iron, Water Res. 45 (2011) 886–892.
[65] Ç. Üzüm, T. Shahwan, A.E. Eroğlu, K.R. Hallam, T.B. Scott, I. Lieberwirth, Synthesis and characterization of kaolinite-supported zero-valent iron nanoparticles and their application for the removal of aqueous Cu^{2+} and Co^{2+} ions, Appl. Clay Sci. 43 (2009) 172–181.
[66] V.S. Mehta, S.K. Chaudhari, Arsenic removal from simulated groundwater using household filter columns containing iron filings and sand, J. Water Proc. Eng. 6 (2015) 151–157.
[67] S. Li, W. Wang, Y. Liu, W.-x. Zhang, Zero-valent iron nanoparticles (nZVI) for the treatment of smelting wastewater: a pilot-scale demonstration, Chem. Eng. J. 254 (2014) 115–123.
[68] W. Yan, A.A. Herzing, C.J. Kiely, W.-x. Zhang, Nanoscale zero-valent iron (nZVI): aspects of the core-shell structure and reactions with inorganic species in water, J. Contam. Hydrol. 118 (2010) 96–104.
[69] A. Jitianu, M. Crisan, A. Meghea, I. Rau, M. Zaharescu, Influence of the silica based matrix on the formation of iron oxide nanoparticles in the Fe_2O_3–SiO_2 system, obtained by sol–gel method, J. Mater. Chem. 12 (2002) 1401–1407.
[70] D. Wen, P. Song, K. Zhang, J. Qian, Thermal oxidation of iron nanoparticles and its implication for chemical-looping combustion, J. Chem. Technol. Biotechnol. 86 (2011) 375–380.
[71] C. Wang, H. Luo, Z. Zhang, Y. Wu, J. Zhang, S. Chen, Removal of As(III) and As(V) from aqueous solutions using nanoscale zero valent iron-reduced graphite oxide modified composites, J. Hazard. Mater. 268 (2014) 124–131.
[72] S.R. Kanel, B. Manning, L. Charlet, H. Choi, Removal of arsenic(III) from groundwater by nanoscale zero-valent iron, Environ. Sci. Technol. 39 (2005) 1291–1298.
[73] C. Han, H. Pu, H. Li, L. Deng, S. Huang, S. He, Y. Luo, The optimization of As(V) removal over mesoporous alumina by using response surface methodology and adsorption mechanism, J. Hazard. Mater. 254–255 (2013) 301–309.
[74] D. Mohan, C.U. Pittman Jr., Arsenic removal from water/wastewater using adsorbents—a critical review, J. Hazard. Mater. 142 (2007) 1–53.
[75] L. Cumbal, J. Greenleaf, D. Leun, A.K. SenGupta, Polymer supported inorganic nanoparticles: characterization and environmental applications, React. Funct. Polym. 54 (2003) 167–180.
[76] B. Babu, S. Gupta, Adsorption of Cr(VI) using activated neem leaves: kinetic studies, Adsorption 14 (2008) 85–92.
[77] D. Mohan, K.P. Singh, V.K. Singh, Wastewater treatment using low cost activated carbons derived from agricultural byproducts—a case study, J. Hazard. Mater. 152 (2008) 1045–1053.
[78] U. Vaid, S. Mittal, J.N. Babu, Removal of hexavalent chromium from aqueous solution using biomass derived fly ash from waste-to-energy power plant, Desalin. Water Treat. 52 (2014) 7845–7855.
[79] G. Suresh Kumar, Mathematical modeling of groundwater flow and solute transport in saturated fractured rock using a dual-porosity approach, J. Hydrol. Eng. 19 (2014) .
[80] A. Milutinović-Nikolić, D. Maksin, N. Jović-Jovičić, M. Mirković, D. Stanković, Z. Mojović, P. Banković, Removal of 99 Tc(VII) by organo-modified bentonite, Appl. Clay Sci. 95 (2014) 294–302.
[81] W. Yan, M.A. Ramos, B.E. Koel, W.-x. Zhang, As(III) sequestration by iron nanoparticles: study of solid-phase redox transformations with X-ray photoelectron spectroscopy, J. Phys. Chem. C 116 (2012) 5303–5311.
[82] W. Yan, R. Vasic, A.I. Frenkel, B.E. Koel, Intraparticle reduction of arsenite (As (III)) by nanoscale zerovalent iron (nZVI) investigated with in situ X-ray absorption spectroscopy, Environ. Sci. Technol. 46 (2012) 7018–7026.
[83] T. Wang, L. Zhang, H. Wang, W. Yang, Y. Fu, W. Zhou, W. Yu, K. Xiang, Z. Su, S. Dai, Controllable synthesis of hierarchical porous Fe_3O_4 particles mediated by poly (diallyldimethylammonium chloride) and their application in arsenic removal, ACS Appl. Mater. Interfaces 5 (2013) 12449–12459.
[84] O.X. Leupin, S.J. Hug, Oxidation and removal of arsenic(III) from aerated groundwater by filtration through sand and zero-valent iron, Water Res. 39 (2005) 1729–1740.
[85] O.X. Leupin, S.J. Hug, A.B.M. Badruzzaman, Arsenic removal from Bangladesh tube well water with filter columns containing zerovalent iron filings and sand, Environ. Sci. Technol. 39 (2005) 8032–8037.
[86] A.B.M. Giasuddin, S.R. Kanel, H. Choi, Adsorption of humic acid onto nanoscale zerovalent iron and its effect on arsenic removal, Environ. Sci. Technol. 41 (2007) 2022–2027.
[87] S. Zhou, D. Wang, H. Sun, J. Chen, S. Wu, P. Na, Synthesis, characterization, and adsorptive properties of magnetic cellulose nanocomposites for arsenic removal, Water Air Soil Pollut. 225 (2014) 1–13.
[88] H. Zhu, Y. Jia, X. Wu, H. Wang, Removal of arsenic from water by supported nano zero-valent iron on activated carbon, J. Hazard. Mater. 172 (2009) 1591–1596.
[89] S. Bhowmick, S. Chakraborty, P. Mondal, W. Van Renterghem, S. Van den Berghe, G. Roman-Ross, D. Chatterjee, M. Iglesias, Montmorillonite-supported nanoscale zero-valent iron for removal of arsenic from aqueous solution: kinetics and mechanism, Chem. Eng. J. 243 (2014) 14–23.